WHITE PAPER

A full-frequency MIMO small-signal model for average current-mode control

flex

Abstract

Designing average current-mode controlled converters is difficult. Many existing models can miss important high-frequency effects or become too cumbersome for practical control design. This paper presents a small-signal frequency-domain model for average current-mode control, developed using the Describing Function method, which captures how the control signal, input voltage, and output voltage each influence inductor-current dynamics. Validated in SIMPLIS and verified on Flex Power Modules' BMR473, the resulting multi-input multi-output (MIMO) model gives engineers a more reliable basis for accurately predicting control-loop stability, audio susceptibility, input/output impedance characteristics, and the onset of sub-harmonic oscillation before hardware is built.

Introduction

Average current-mode control is widely used in switching converters, but modeling its behavior across the full frequency range is not common or straightforward. For design engineers, that gap in behavior modeling matters because the missing behavior is often where stability problems, noise sensitivity, and sub-harmonic oscillation begin to show up. Earlier approaches each solved part of the problem, but none were comprehensive. In one of the earliest approaches [1], peak current-mode control is represented by modeling the inductor current as a controlled current source, offering intuitive physical insight. However, this approach lacks the fidelity needed to predict sub-harmonic oscillations. Ridley's model [2] addresses this limitation by capturing the sample-and-hold behavior of the inductor current, which becomes critical when the duty cycle exceeds 50%. Despite its accuracy, Ridley's method is not easily extendable to modern control schemes. To overcome these limitations, the Describing Function method [3] was introduced as a versatile modeling approach. It has been successfully applied to constant-frequency peak current-mode control, constant on/off-time controls, and was extended to V^2 control [4].

The first application of the Describing Function method to average current-mode control was presented soon after [5], along with its equivalent circuit representation [6]. While these works provided a thorough analysis of the control loop, they did not fully address other critical transfer functions.

This paper proposes a multi-input multi-output (MIMO) model for average current-mode control. The model enables comprehensive analysis and synthesis of both the inner current loop and the outer voltage loop, while also capturing key system characteristics including loop stability, audio susceptibility, and impedance behavior up to the switching frequency. This facilitates accurate prediction and mitigation of sub-harmonic oscillations, contributing to more robust designs.

Modeling of the current loop in average current mode control

Fig. 1a shows a typical average current-mode control implemented using an Operational Transconductance Amplifier (OTA) where v_{com} is expressed by the first part of (1) utilizing the method described in [6], i.e., rewrite the control signal into two parts: one without dynamics and one with dynamics, as is shown in the last part of (1).

$$v_{com} = \left(R_z + \frac{1}{sC_z}\right) g_m(v_c - R_i i_L) = -R_z g_m R_i i_L + \frac{1}{sC_z} g_m[-R_i i_L + (1 + sR_z C_z)v_c] \tag{1}$$

This is illustrated in Fig. 1b, where we have an inner peak current feedback loop with the sense resistance $R_s = R_z g_m R_i$, and the outer loop with the sense resistance R_i. The OTA's input current, (with transconductance g_m), feeds the capacitor C_z, yielding an integrator, $H_I = g_m/sC_z$, and the control signal v_c is filtered with $H_C = 1 + sR\ C$.

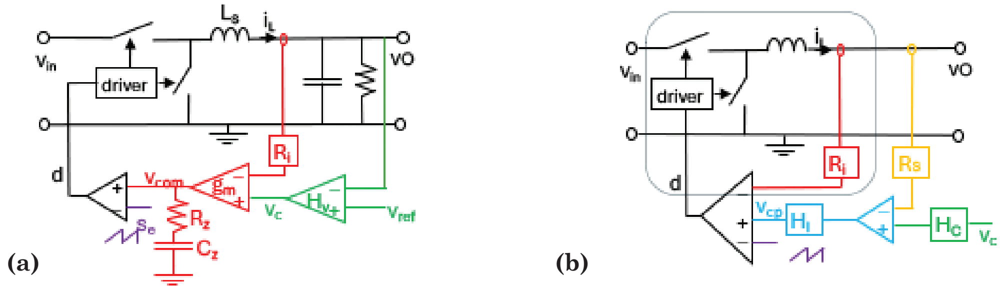

Figure 1: (a) Average Current-Mode Control with OTA, (b) Separation into two current feedback loops.

The control to inductor transfer function $H_{cp} = i_L(s)/v_c(s)|_{peak}$ was previously derived in [3], here we substitute the sense resistance R_i with the amplified R_s. The full frequency and the simplified transfer functions yields:

$$H_{cp} = \left.\frac{i_L(s)}{v_c(s)}\right|_{peak} = \frac{V_{in}}{sT_{sw}L_s} \frac{1-e^{-sT_{sw}}}{(s_n+s_e)+(s_f-s_e)e^{-sT_{sw}}} \approx \frac{1}{R_s} \frac{\omega_2^2}{s^2+s\frac{\omega_2}{Q_2}+\omega_2^2}. \tag{2}$$

Using the definitions from [3], $\omega_2 = \frac{\pi}{T_{sw}},\ Q_2 = \frac{1}{\pi\left[\frac{s_n+s_e}{s_n+s_f}-0.5\right]}$

where T_{sw} is the switch period . The inductors' rising and falling current slopes are, $s_n = R_s\frac{V_{in}-V_{out}}{L}$, and $s_f = R_s\frac{V_{out}}{L}$

, respectively. The compensation ramp slope is denoted s_e, which can be used to design the Q_2 value in (2). The simplified model, which is accurate up to the Nyquist frequency, is obtained using a Pade approximation of the time delay, $e^{-sT_{sw}}$ [3].

The peak current control to inductor transfer function, $i_L(s)/v_c(s)|_{peak}$ in (2), is fed-back with the outer current loop, as illustrated in Fig. 1b, via the sense resistor R_i, and integrator H_I, which yields the control to inductor current transfer function for average current-mode control:

$$\left.\frac{i_L(s)}{v_c(s)}\right|_{avg} = \frac{H_I(i_L(s)/v_c(s)|_{peak})}{1+R_iH_I(i_L(s)/v_c(s)|_{peak})} H_c \tag{3}$$

Through algebraic manipulation of (3), both the full and simplified models are derived as follows:

$$\left.\frac{i_L(s)}{v_c(s)}\right|_{avg} = \frac{V_{in}g_m\left(1-e^{-sT_{sw}}\right)(1+s/n_Z)}{s^2T_{sw}L_sC_Z\left((s_n+s_e)+(s_f-s_e)e^{-sT_{sw}}\right)+R_iV_{in}g_m\left(1-e^{-sT_{sw}}\right)} \approx \frac{\omega_2^2}{R_i}\frac{s+n_Z}{s^3+s^2\frac{\omega_2}{Q_2}+s\omega_2^2+n_Z\omega_2^2}. \tag{4}$$

The outer current loop with the integrator introduces a zero, $n_z = \frac{1}{C_z R_z}$, as well as an additional pole. This configuration also influences the placement of the two poles associated with the inner peak current control loop. A comprehensive stability analysis of this configuration is provided in [6]. The models in (4) are verified with SIMPLIS simulations and shown in Fig. 2. The following data was used: Switching frequency f_{sw}=300 kHz, V_{in}=12 V, V_{out}=6 V, L_s=300 nH, g_m=0.85mS, s_e=0.8s_f, and f_z=f_{sw}/10=30kHz. With R_z=1kΩ, the capacitor becomes $C_z = \frac{1}{2\pi R_z f_z} = 5.3nF$

The correspondence between the full frequency model and the simulation is very good for the gain, while the phase starts to deviate at 600 kHz. The simplified model has very good agreement up to the Nyquist frequency.

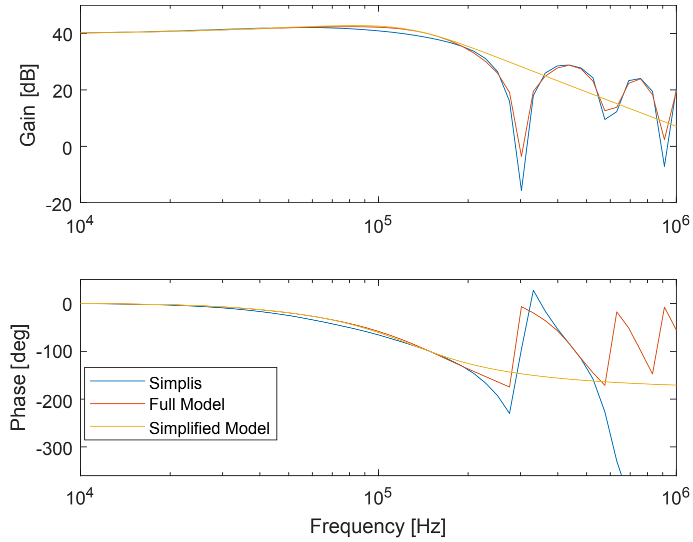

Figure 2: Control to i_L transfer function comparison and verification with SIMPLIS simulation.

Input and output voltage to inductor current transfer functions

To be able to analyze all the other transfer functions the input and output voltage to inductor current transfer functions are required. Using the structure from [3] for the MIMO model of the inductor current shown in Fig. 4, where $i_L(s)/v_c(s)|_{avg}$ serves as a common component across all three transfer functions, yields $\left.\frac{i_L(s)}{v_{in}(s)}\right|_{avg} = K_1\left.\frac{i_L(s)}{v_c(s)}\right|_{avg}$, and $\left.\frac{i_L(s)}{v_{out}(s)}\right|_{avg} = K_2\left.\frac{i_L(s)}{v_c(s)}\right|_{avg}$ Solving for K_1, and K_2, yields:

$$K_1 = \frac{i_L(s)/v_{in}(s)|_{avg}}{i_L(s)/v_c(s)|_{avg}},\ K_2 = \frac{i_L(s)/v_{out}(s)|_{avg}}{i_L(s)/v_c(s)|_{avg}}. \tag{5}$$

The transfer functions $i_L(s)/v_{in}(s)|_{avg}$, and $i_L(s)/v_{out}(s)|_{avg}$ are determined by the feedback of the outer current loop, incorporating the term $H_I R_i$, see Fig. 1b. The following relationships are obtained:

$$K_1 = \frac{\dfrac{\left(i_L(s)/v_{in}(s)|_{peak}\right)}{1+H_I R_i\left(i_L(s)/v_{in}(s)|_{peak}\right)}}{i_L(s)/v_c(s)|_{avg}}, \; K_2 = \frac{\dfrac{\left(i_L(s)/v_{out}(s)|_{peak}\right)}{1+H_I R_i\left(i_L(s)/v_{out}(s)|_{peak}\right)}}{i_L(s)/v_c(s)|_{avg}}. \tag{6}$$

Where $i_L(s)/v_{in}(s)|_{peak}$, and $i_L(s)/v_{out}(s)|_{peak}$ are found in [3] as

$$\left.\frac{i_L(s)}{v_{in}(s)}\right|_{peak} = \frac{1}{sL_s T_{sw}}\left[-\frac{1}{(s_n+s_e)+(s_f-s_e)e^{-sT_{sw}}}\frac{1-e^{-sT_{on}}}{sL_s/R_s}V_{in} + T_{on}\right], \left.\frac{i_L(s)}{v_{out}(s)}\right|_{peak} = \frac{1}{sL_s}\left[\frac{f_s\left(1-e^{-sT_{sw}}\right)}{(s_n+s_e)+(s_f-s_e)e^{-sT_{sw}}}\frac{1}{sL_s/R_s}V_{in} - T_{sw}\right] \tag{7}$$

Since $1 \gg H_I R_i i_L(s)/v_{in}(s)|_{peak}$ (here at least 20dB smaller), and the DC gains of $i_L(s)/v_c(s)|_{avg}$ and $i_L(s)/v_c(s)|_{peak}$ are identical, one can approximate K_1 as in (8).

$$K_1 = \frac{\dfrac{\left(i_L(s)/v_{in}(s)|_{peak}\right)}{1+H_I R_i\left(i_L(s)/v_{in}(s)|_{peak}\right)}}{i_L(s)/v_c(s)|_{avg}} \approx \frac{i_L(s)/v_{in}(s)|_{peak}}{i_L(s)/v_c(s)|_{peak}} \approx \frac{DR_i}{L}\left[\frac{1}{Q_2\omega_2} - \frac{T_{off}}{2}\right], \; K_2 \approx -\frac{R_i}{LQ_2\omega_2} \tag{8}$$

The same line of reasoning can be applied to K_2. The results match those observed in the peak current control mode scenario in [3]. The full (6) and simplified models (8) of K_1 are compared in Fig. 3a. The simplified K_1 model is verified with SIMPLIS simulation and compared with the calculated $i_L(s)/v_{in}(s)|_{avg} = K_1 i_L(s)/v_c(s)|_{avg}$, which is shown in Fig. 3b. Both these comparisons show excellent similarities up to the Nyquist frequency.

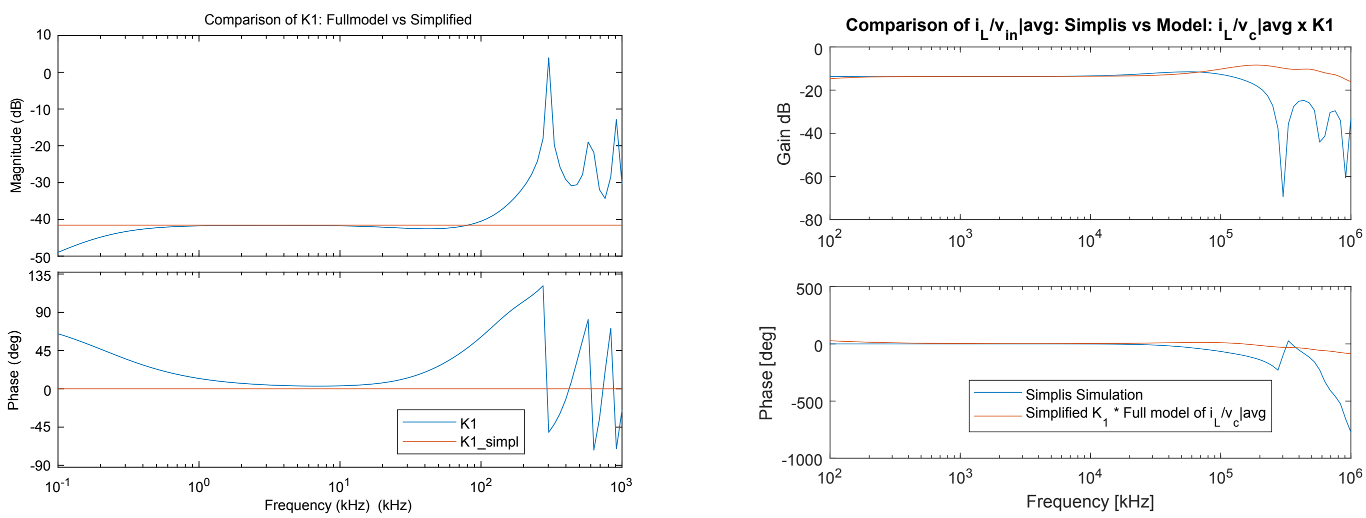

Figure 3: a) V_{in} to i_L transfer functions, Fullmodel vs Simplified. b) Verification of K_1 with SIMPLIS

The average current-mode model

The average current-mode model is applied in Fig. 4b. The MIMO model of the inductor current i_L in Fig. 4a, feeds an impedance network, Z_{out}, in series with the inductor's parasitic resistance DCR. The voltage at the inductors' output is fed back via K_2. The control to output voltage transfer function for peak current-mode control was previously derived in [7]. By substituting with the average current-mode control expression given in equation (4), the equivalent for average current-mode control is obtained as

$$\left.\frac{v_{out}(s)}{v_c(s)}\right|_{avg} = \frac{Z_{out}\left(i_L(s)/v_c(s)|_{avg}\right)}{1-K_2(DCR+Z_{out})\left(i_L(s)/v_c(s)|_{avg}\right)} \tag{9}$$

With (9) established, the voltage control loop can now be closed. A PID controller is then designed to meet the desired stability criteria. Subsequently, all the key system performance metrics can be analyzed.

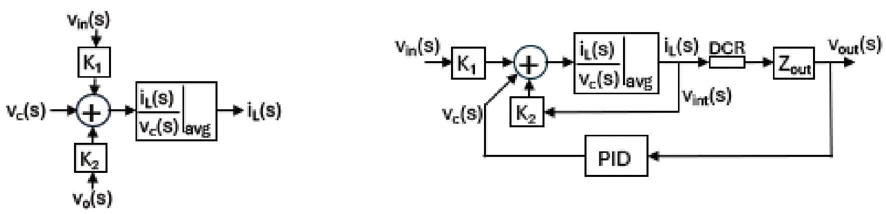

(a) (b)

Figure 4: (a) The MIMO model of the inductor current and (b) its use in the full model of the SMPS.

Implementation and verification

A suitable control circuit implementing the average current control with an OTA is the TPS546A24A from Texas Instruments [8]. This was successfully introduced in the 40A non-isolated digital PoL Regulator, BMR473 [9]. Within the Flex Power Designer Loop Compensation Tool, the verified model supports control-loop design as well as load-transient analysis for the output decoupling capacitor bank. That gives the work a practical endpoint. It is not only mathematically consistent, but directly usable in day-to-day converter design.

Conclusions

A linear time-invariant MIMO small-signal model for average current-mode control has been developed using the Describing Function method. This approach captures the full frequency content of the highly nonlinear current loop, enabling accurate analysis up to the switching frequency. As a result, the model facilitates early detection and mitigation of sub-harmonic oscillations during the design phase. By combining the inner peak-current loop and the outer average-current loop in one framework, it provides a more complete account of how the control signal, input voltage, and output voltage influence inductor-current behavior. This allows stability issues to be identified earlier, gives a better basis for controller design and reduces the risk of sub-harmonic oscillation reaching hardware. The model has been validated through SIMPLIS simulations, verified with measurements on the Flex Power Modules product BMR473, and implemented in the Flex Power Designer Loop Compensation Tool for practical use. For power designers, the value is straightforward: a model that stays mathematically rigorous while being more useful in practice.

References

[1] S. P. Hsu, A. Brown, L. Rensink, and R. D. Middlebrook, "Modeling and analysis of switching dc-to-dc converters in constant-frequency current programmed mode," *in Proc. IEEE PESC 1979*, pp. 284–301.

[2] R. B. Ridley, "A new, continuous-time model for current-mode control," *IEEE Transactions on Power Electronics*, vol. 6, no. 2, pp. 271-280, April 1991.

[3] J. Li and F. C. Lee, "New modeling approach and equivalent circuit representation for current-mode control," *IEEE Trans. Power Electronics*, vol. 25, no. 5, pp. 1218–1230, May 2010.

[4] J. Li and F. C. Lee, "Modeling of V^2 Current-Mode Control," *IEEE Transactions on Power Electronics*, vol. 57, no. 9, pp. 2552-2563, Sept. 2010.

[5] F. Yu, F. C. Lee, and P. Mattavelli, "A small signal model for average current-mode control based on describing function approach," *2011 IEEE Energy Conversion Congress and Exposition*, Phoenix, AZ, USA, 2011, pp. 405-412.

[6] Y. Yan, F. C. Lee, and P. Mattavelli, "Analysis and Design of Average Current-Mode Control Using a Describing-Function-Based Equivalent Circuit Model," *IEEE Transactions on Power Electronics*, vol. 28, no. 10, pp. 4732-4741, Oct. 2013.

[7] J. Li, "Current-Mode Control: Modeling and its Digital Application", Ph.D. dissertation, Dept. of Electrical and Computer Engineering, Virginia Polytechnic Institute and State University, Blacksburg, VA, USA, 2009.

[8] Texas Instruments, "TPS546A24A 2.95-V to 18-V, stackable 10-A synchronous SWIFT™ buck converter with pin-strapping and PMBus," TI.com. https://www.ti.com/product/TPS546A24A

[9] Flex Power Modules, "BMR473 series." Available: https://flexpowermodules.com/products/bmr473. Published: Jun. 14, 2022. Accessed: Mar. 4, 2026.

Connect with us

pm.info@flex.com

flex.com/products/power-modules

flexpowerdesigner.com

linkedin.com/showcase/flex-power-modules

flex.com/products/power-modules/wechat

youtube.com/flexintl